Sensors and Materials, Vol. 36, No. 10 (2024) 4253–4268
MYU Tokyo

S & M 3798

Applying Fuzzy Theory to Enhance the Longitudinal Control of Miniaturized Electric Unmanned Aerial Vehicles

Chao-Pang Wu,[1] Nan-Kai Hsieh,[2*] and Liang-Rui Chen[1]

[1]Department of Electrical Engineering, National Changhua University of Education,
No. 1, Jinde Rd., Changhua City, Changhua County 50007, Taiwan
[2]Department of Automatic Control Engineering, Feng Chia University,
No. 100, Wenhua Rd., Xitun Dist., Taichung City 407102, Taiwan

(Received May 24, 2024; accepted September 2, 2024)

Keywords: unmanned aerial vehicle (UAV), PID control, fuzzy theory, DATCOM, Simulink

In recent years, micro-sized electric unmanned aerial vehicle (UAVs) have gained widespread applications in both defense and civilian sectors owing to their advantages of lightweight construction, portability, and cost-effectiveness. However, a significant drawback is the difficulty in discerning and controlling the flight attitude and trajectory of these UAVs when operating beyond the line of sight. Consequently, they heavily rely on remote control for flight operations, leading to a high degree of operational complexity. Hence, it is challenging to maintain the desired characteristics of micro-sized aerial vehicle systems, such as high sensitivity and stability. In this study, we aimed to enhance the longitudinal flight stability of micro-sized electric UAVs. To achieve this goal, control of a UAV's elevator was utilized to ensure stability in pitch and roll during flight. We employed the Digital Airborne Tactical Communications System (DATCOM) software developed by the United States Air Force to calculate the fundamental aerodynamic coefficients of the UAV. Subsequently, the longitudinal motion state space equation was employed to derive transfer functions for the pitch angle θ and the horizontal stabilizer deflection δe. Furthermore, we utilized Simulink to compare the effects of two control methods, traditional Proportional-Integral-Derivative (PID) and fuzzy PID, on the longitudinal flight stability of the UAV. We aimed to identify the optimal PID values for the UAV. Finally, we validated through practical flight tests that Fuzzy PID can enhance the longitudinal flight stability of the UAV while also contributing to new technological solutions for stability in micro-sized UAV flight.

1. Introduction

Unmanned aerial vehicle (UAVs) can generally be classified into two main categories on the basis of their physical configurations: fixed wing and multirotor.(1) The UAV utilized in this study is a fixed-wing UAV with a weight of 1.25 kg and a wingspan of 140 cm, categorizing it as a micro-sized electric UAV. The advantages of the micro-sized UAV include the following: (1)

*Corresponding author: e-mail: nkhsieh@fcu.edu.tw
https://doi.org/10.18494/SAM5155

ISSN 0914-4935

compact size, portability, and high maneuverability and (2) the utilization of lightweight lithium polymer (Li–Po) batteries for UAV power, known for their high efficiency and easy availability.[2,3] On the other hand, the disadvantages of the micro-sized electric UAV include the following: (1) during long-distance flights, it becomes challenging to visually control the UAV's flight attitude owing to its small size. As a result, it is necessary to control and operate the UAV through Beyond Visual Line of Sight. (2) Micro-sized UAVs exhibit a relatively smaller aspect ratio than their larger counterparts, resulting in lower lift coefficients that can impact flight stability. Consequently, the optimization of flight control computer parameters is essential for real-time adjustments to the UAV's flight attitude to maintain stability. Therefore, the UAV's control system must be a rapid-response system to mitigate concerns related to flight safety or the risk of crashes. Thus, the primary objective of this research is to explore methods for enhancing the flight stability of UAVs.

Methods for optimizing the flight stability of UAVs include various control techniques such as ant colony optimization,[4] neural network optimization, fuzzy control,[5] and particle swarm optimization. These control techniques have demonstrated successful applications in the dynamic flight control systems of UAVs.[6] This has led to an increasing number of research endeavors aimed at integrating algorithms with conventional control methods to simplify complex control systems and significantly enhance small-scale control systems' stability. In general, the exploration of flight stability in UAVs often begins with the traditional PID controller as the primary focus.[7,8] Its advantage lies in its simplicity of construction, but it is only suitable for linear systems. Additionally, the three parameters (*P*, *I*, and *D*) must be precisely calculated for the system; otherwise, iterative adjustments are required until the desired performance is achieved. When applied to nonlinear systems, it may not meet system requirements and could potentially lead to system instability. In this research, we employed a fuzzy controller in conjunction with the PID method to control the longitudinal stability of a UAV. A fuzzy controller is a type of nonlinear control system that is easily manageable and comprehensible. It offers superior adaptability and robustness, as well as fault tolerance. This technology can dynamically adjust output-based controller parameters, utilizing fuzzy logic and inference rules to modify controller settings. Fuzzy theory was based on rough information patterns for subjectively categorizing human data, whereas traditional control systems require precise mathematical models for processing. However, establishing a precise mathematical system often demands a significant investment of human and material resources to meet the required standards. The advantage of fuzzy theory lies in its ability to address difficulties in acquiring mathematical models and in handling the complex dynamics of aircraft, which are often challenging to control. Therefore, fuzzy theory attempts to simplify the complexity of problems by adopting a human thinking approach and can achieve results similar to traditional control methods. As such, fuzzy theory is considered one of the effective approaches for enhancing traditional PID controllers.[9,10] Fuzzy control systems inherently possess a degree of adaptability and robustness, allowing for real-time adjustments and responsiveness to the UAV's flight status changes. Levina *et al.*[11] proposed using traditional PID control and validated its effectiveness in enhancing flight stability through simulations. In contrast, Chu *et al.*[12] and Yan *et al.*[13] conducted studies on flight simulation using fuzzy PID. Therefore, to verify the effectiveness of fuzzy PID in improving the flight stability of fixed-wing UAV, we first validated

the effectiveness of both traditional PID and fuzzy PID in enhancing flight stability through simulations. Subsequently, a comparison was made with the actual flights using fuzzy logic conducted by Sun *et al.*[14] Finally, we demonstrated through both simulated and actual flight results that fuzzy PID can enhance the longitudinal flight stability of fixed-wing UAVs. This capability enhances the longitudinal control performance and stability of micro-sized electric UAVs and offers broader possibilities for applications in fields such as agriculture, mapping, and disaster rescue.[15,16]

2. Research Method

2.1 Introduction to UAV longitudinal motion state space equation

According to the flight control theory, the longitudinal attitude control of a UAV primarily involves pitch angle and altitude control. A common control approach employs the elevator to achieve the longitudinal attitude of the UAV. The longitudinal control system of the UAV involves the vertical motion of the aircraft, including climbing and descending. When designing longitudinal control, Euler angles and altitude are typically used as input variables to control the vertical motion of the aircraft. The motion model of the UAV is illustrated in Fig. 1.

On the basis of the aerodynamic data and flight conditions of the unmanned aerial vehicle under certain conditions, the longitudinal motion state space equation of the UAV is determined

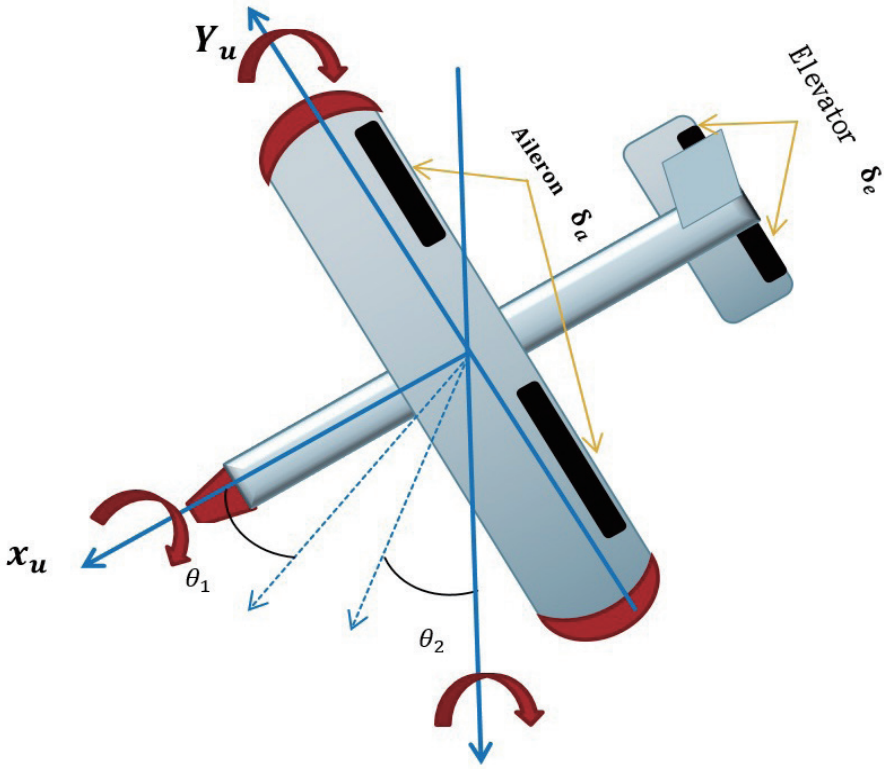

Fig. 1. (Color online) UAV motion model.

by calculating the parameters of the UAV's longitudinal motion state equation, as shown in Eq. (1): $\dot{X}$ represents the UAV's longitudinal motion state space equation, where A and B are matrices as described in Eqs. (2) and (3), x is the state vector as defined in Eq. (4), and η is the control vector as shown in Eq. (5).

$$\dot{X} = Ax + B\eta \tag{1}$$

$$A = \begin{bmatrix} X_u & X_w & 0 & -g \\ Z_u & Z_w & Z_q + u_0 & 0 \\ M_u + M_{\dot{w}} Z_u & M_w + M_{\dot{w}} Z_w & M_q + M_{\dot{w}} u_0 & 0 \\ 0 & 0 & 1 & 0 \end{bmatrix} \tag{2}$$

$$B = \begin{bmatrix} X_{\delta_E} \\ Z_{\delta_E} \\ M_{\delta_E} + M_{\dot{w}} Z_{\delta_E} \\ 0 \end{bmatrix} \tag{3}$$

$$x = \begin{bmatrix} \Delta u \\ \Delta w \\ \Delta q \\ \Delta \theta \end{bmatrix} \tag{4}$$

$$\eta = \left[\delta_E\right] = K_P e(t) + K_i \int e(t)\,dt + K_d \frac{de(t)}{dt} \tag{5}$$

In this study, we employed DATCOM[17,18] to analyze the aerodynamic coefficients of the aircraft. Developed by the United States Air Force, DATCOM is a computer program utilized for conducting aerodynamic analysis and predicting various aircraft properties.

The DATCOM software requires the input of various parameters of the aircraft, such as wing geometry, fuselage shape, control surfaces, flight altitude, and velocity. These inputs are utilized to estimate coefficients such as lift, drag, and pitching moment, which are essential for analyzing and predicting the aircraft's performance, stability, and control characteristics.

The UAV utilized in this study, as depicted in Fig. 2, exhibits various geometric parameters, including external dimensions and weight, which are shown in Table 1. We input the measurement data into DATCOM, calculate the basic aerodynamic coefficient of the UAV (Table 2), and substitute it into Formula for the longitudinal moment of UAV (Table 3) and Eqs. (1)–(5) to calculate the longitudinal state space matrix of the UAV, as shown in Eq. (6). Using the Laplace transform, we derived the transfer functions of the pitch angle θ and the horizontal stabilizer deflection δe as shown in Eq. (7).

Fig. 2. (Color online) Micro-sized UAV.

Table 1
Geometric parameters of micro-sized electric UAV.

Parameter	Value	Unit
Wingspan	140	cm
Wing chord length	22	cm
Wing area	3080	cm^2
Horizontal tail wingspan	45	cm
Horizontal tail chord length	12	cm
Horizontal tail area	540	cm^2
Vertical tail length	19	cm
Vertical tail chord length	13	cm
Vertical tail area	247	cm^2
Fuselage length	86	cm
Total aircraft weight	1.25	kg
Maximum cruise speed (V)	13	m/s

Table 2
DATCOM longitudinal coefficient of UAV.

Parameter	Value	Parameter	Value
C_{D_0}	0.051	X_u	−0.2634
C_{D_u}	0	Z_u	−1.608
C_{l_u}	0	M_u	0
C_{l_0}	0.467	X_w	0.804
C_{D_α}	0	Z_w	−8.6466
C_{m_u}	0	M_w	−3.6553
C_{m_α}	−0.671	X_α	8.4417
C_{l_α}	4.9715	Z_α	−90.7894
$C_{m_{\delta e}}$	−0.7921	M_α	−38.3804
$C_{l_{\delta e}}$	0.2996	$X_{w\cdot}$	0
C_{l_q}	4.1858	$Z_{w\cdot}$	0
C_{m_q}	−7.449	$M_{w\cdot}$	−0.1699
$C_{m_{\dot\alpha}}$	−3.1744	$X_{w\cdot}$	0
$C_{D_{\delta e}}$	0.0225	$Z_{\dot\alpha}$	0
X_q	0	$M_{\dot\alpha}$	−1.7842

Table 3
Formula for longitudinal moment of UAV.

X-axis moment	*Z*-axis moment	Pitching moment
$X_u = -\frac{QS}{mu_0}\left(C_{D_u} + 2C_{D_0}\right)$	$Z_u = -\frac{QS}{mu_0}\left(C_{L_u} + 2C_{L_0}\right)$	$M_u = C_{m_u}\frac{QS\overline{c}}{u_0 I_y}$
$X_w = -\frac{QS}{mu_0}\left(C_{D_\alpha} + C_{L_0}\right)$	$Z_w = -\frac{QS}{mu_0}\left(C_{L_\alpha} + C_{D_0}\right)$	$M_w = C_{m_\alpha}\frac{\left(QS\overline{c}\right)}{u_0 I_y}$
	$Z_{\dot{w}} = C_{Z_{\dot{\alpha}}}\frac{\overline{c}}{2u_0}\frac{QS}{u_0 m}$	$M_q = C_{m_q}\frac{\overline{c}}{2u_0}\frac{QS\overline{c}}{I_y}$
	$Z_q = C_{Z_q}\frac{\overline{c}}{2u_0}\frac{QS}{m}$	$M_{\dot{w}} = C_{m_{\dot{\alpha}}}\frac{\overline{c}}{2u_0}\frac{QS\overline{c}}{u_0 I_y}$
	$Z_{\delta_E} = C_{Z_{\delta_E}}\frac{QS}{m}$	$M_{\delta_E} = C_{m_{\delta_E}}\frac{QS\overline{c}}{I_y}$

$$\begin{bmatrix}\dot{u}\\ \dot{w}\\ \dot{q}\\ \dot{\theta}\end{bmatrix} = \begin{bmatrix}-0.2634 & 0.8040 & 0 & -9.81\\ -1.6080 & -8.6466 & 10.5 & 0\\ 0.2732 & -2.1860 & -5.9708 & 0\\ 0 & 0 & 1 & 0\end{bmatrix}\cdot\begin{bmatrix}u\\ w\\ q\\ \theta\end{bmatrix} + \begin{bmatrix}-0.4067\\ -6.6341\\ 0.1180\\ 0\end{bmatrix}\left[\delta e\right] \tag{6}$$

$$\frac{\theta}{\delta e} = \frac{-1.802s^3 - 35.17s^2 + 41.65s - 107}{s^4 + 20.03s^3 + 29.22s^2 + 335.4s - 9.338} \tag{7}$$

2.2 Structure and design of fuzzy-PID control system

In this study, the longitudinal pitch angle error *e* and the error rate of change ec of the UAV are taken as the input values $r(t)$ for the controller. The actual output value is represented as $y(t)$, and $u(t)$ denotes the output signal. Here, 't' indicates the parameter of time. By constructing a fuzzy theory knowledge base and a rule base, we can make the PID controller of the UAV undergo fuzzification to determine the values of K_P, K_i, and K_d. Through the Fuzzy-PID control system structure, as illustrated in Fig. 3, the controlled object (UAV) achieves enhanced adaptability and robustness.

The PID parameters of this control system are given by Eq. (8).

$$\begin{cases} K_P = K_{P0} + \Delta K_P \\ K_i = K_{i0} + \Delta K_i \\ K_d = K_{d0} + \Delta K_d \end{cases} \tag{8}$$

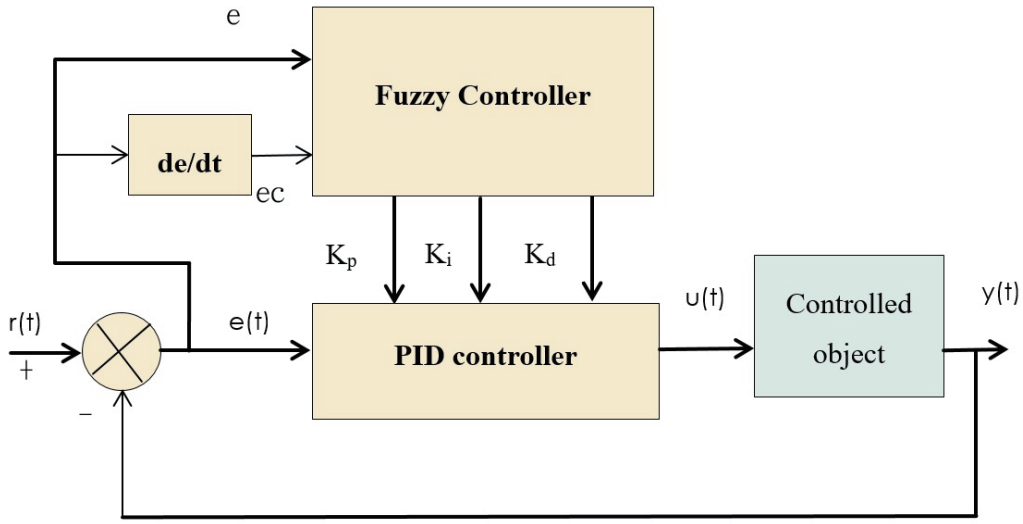

Fig. 3. (Color online) Fuzzy-PID control system structure.

Among these, K_{P_0}, K_{i_0}, and K_{d_0} represent the initial values for the proportional, integral, and derivative coefficients, respectively. ΔK_P, ΔK_i and ΔK_d denote the output values of the fuzzy controller, while K_P, K_i, and K_d represent the final system output values.

According to PID theory,[19,20] it is highlighted within PID controllers that the configuration, adjustment, and optimization of the three-parameter sets K_P, K_i and K_d are considerably reliant on the experiences of researchers and experts. The relevant experiences are as follows.

K_P (Proportional Gain): This is the initial component of the PID controller. It determines the control response on the basis of the error signal, which represents the difference between the desired setpoint and the actual measured value. A higher value of K_P leads to a more pronounced response to the error; however, if set too high, it may result in excessive overshoot and instability.

K_i (Integral Gain): This is the second component of the PID controller that considers the accumulated sum of past errors over time. It helps eliminate potential steady-state errors and enables the controller to handle situations where a constant deviation exists between the setpoint and the actual value.

K_d (Derivative Gain): This is the third component of the PID controller. It considers the rate of change of the error signal over time. By utilizing this information, the controller can predict future errors and respond in advance, aiding in reducing maximum overshoot and enhancing the stability and responsiveness of the control system.

In conventional control systems, the PID controller is extensively utilized for regulating the dynamic responses of stable systems. In the design of PID controllers, a critical concept is the "stability region", which refers to the range of controller parameters within which the closed-loop response of the system remains stable. The methods commonly employed for computing the stability region of PID controllers include root locus analysis, Bode plot analysis, and Nyquist plot analysis. All of these methods can be utilized to determine the stability region of a PID controller.

To achieve faster and more precise convergence of PID control, we utilized the method for calculating the stability region of the PID controller as proposed by Tan *et al.*[21] By applying Eq. (7) and utilizing Eqs. (9)–(12), we determined the values of K_P, K_i, and K_d[21–23] within the stability range, which served as the preliminary combination for designing the PID controller's stability region, as shown in Fig. 4. This approach, employing stability boundary trajectory analysis and the rapid identification of suitable parameter adjustments, facilitates a method for achieving the faster convergence of PID parameters.

In this study, to achieve faster and more accurate convergence of the PID controller, we employed the approach proposed by Tan *et al.*[21] for calculating the stability region of the PID controller. The transfer function from Eq. (7) was transformed using Eqs. (9)–(12) to compute the stable ranges of K_P, K_i, and K_d.[17,18] These ranges were then utilized to determine the preliminary combination of PID controller design for achieving stability, as shown in Fig. 4. Fuzzy PID utilizes the stability boundary locus method to compute and rapidly identify the necessary model for appropriate parameter adjustments, providing a method to expedite the convergence of PID parameters.

$$G(j\omega)=\frac{B_E(-\omega^2)+j\omega B_0(-\omega^2)}{A_E(-\omega^2)+j\omega A_0(-\omega^2)} \tag{9}$$

$$K_p(\omega,k_D)=\frac{P_5(\omega)P_4(\omega)-P_6(\omega)P_2(\omega)}{P_1(\omega)P_4(\omega)-P_2(\omega)P_3(\omega)} \tag{10}$$

$$K_p(\omega,k_D)=\frac{P_6(\omega)P_1(\omega)-P_5(\omega)P_3(\omega)}{P_1(\omega)P_4(\omega)-P_2(\omega)P_3(\omega)} \tag{11}$$

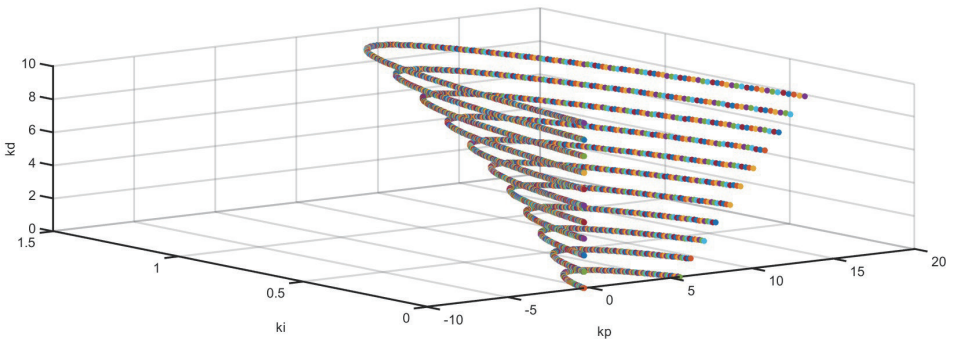

Fig. 4. (Color online) Ranges of K_P, K_i, and K_d.

$$\begin{cases} P_1(\omega) = -\omega^2 B_0\left(-\omega^2\right) \\ P_2(\omega) = B_E\left(-\omega^2\right) \\ P_3(\omega) = \omega B_E\left(-\omega^2\right) \\ P_4(\omega) = \omega B_0\left(-\omega^2\right) \\ P_5(\omega) = \omega^2 A_0\left(-\omega^2\right) + \omega^2 B_E\left(\omega^2\right) k_D \\ P_6(\omega) = -\omega A_E\left(-\omega^2\right) + \omega^3 B_0\left(-\omega^2\right) k_D \end{cases} \tag{12}$$

The region where the controller parameters for feedback stability can be placed is obtained by plotting the stability boundary locus of the controlled object. From expert experience, the variations in PID gains are influenced by different combinations of $|e|$ and $|ec|$ as follows.

(1) When $|e|$ varies, the principles for adjusting the PID parameters K_P, K_i, and K_d are as follows.
   (a) When the value of $|e|$ is large, a larger K_P value is chosen to accelerate the response speed, along with an appropriate K_d value. Typically, for larger values of $|ec|$, a larger K_d value is adopted, and for smaller values of $|ec|$, a comparatively smaller K_P value is chosen. To prevent integral windup and avoid the occurrence of maximum overshoot in the system response, a smaller K_i value should be taken.
   (b) When the value of $|e|$ is moderate, in order to mitigate the maximum overshoot in the system response, K_P, K_i, and K_d should not be excessively large. At this point, moderate K_P and K_d values should be chosen along with a relatively smaller K_i value, ensuring a balanced system response speed.
   (c) When the value of $|e|$ is small, the values of K_P and K_i should be increased to achieve excellent steady-state characteristics. Simultaneously, to prevent system oscillations near the setpoint, an appropriately smaller K_d value should be selected.

(2) When $|ec|$ varies, the principles for adjusting the PID parameters K_P, K_i, and K_d are as follows.
   (a) When $|ec|$ is relatively large, the values of K_P, K_i, and K_d should not be too large. K_P should be selected from a relatively small to moderate range, K_i should be kept as small as possible while considering the inherent control characteristics of the system, and K_d should be chosen to be relatively large.
   (b) When $|ec|$ is moderate, to accelerate the system's response speed and achieve favorable steady-state characteristics, it is advisable to increase the values of K_P and K_i. To prevent output response oscillations near the setpoint and considering the system's resistance to disturbances, a relatively smaller value of K_P should be chosen to ensure system stability.
   (c) When the value of $|ec|$ is small, in order to ensure a faster response of the system, it is advisable to increase the values of K_P and K_i. Simultaneously, considering the system's resistance to disturbances, an appropriate K_d value should be selected.

2.3 Determining membership functions and fuzzy rules

Drawing upon the fuzzy set theory,[24] we transformed input and output values into linguistic variables, a process termed fuzzification. The input variables e and ec fall within the range ϵ [−5, 5], whereas the output variables K_P, K_i, and K_d constitute three sets with the range ϵ [−5, 5]. The fuzzy range for input and output values is categorized into seven linguistic variables, corresponding to the following fuzzy subsets:

$$e, ec = \text{NB, NM, NS, ZO, PS, PM, PB,}$$
$$K_P, K_i, \text{ and } K_d = \text{NB, NM, NS, ZO, PS, PM, PB.}$$

These linguistic variables correspond to the following fuzzy subsets: NB (Negative Big), NM (Negative Middle), NS (Negative Small), ZO (Zero), PB (Positive Big), PM (Positive Middle), and PS (Positive Small).

Common defuzzification methods include the center of area (COA) or the center of gravity (COG), the mean of maximum (MOM), and the center of sums (COS).[25] In this study, the commonly used COG method was employed for calculation, as shown in Eq. (13).

$$y^0 = \frac{\int y \mu b(y) y dy}{\int y \mu b(y) dy} \tag{13}$$

After defuzzification, the output values were scaled by a proportionality factor to obtain the practical application values. Building upon the aforementioned *P*, *I*, and *D* parameters, we adapted Eq. (13) to meet the desired ratio requirements for various error *e* and error change ec values. Subsequently, the ΔK_P, ΔK_i, and ΔK_d fuzzy rules were computed and organized, as presented in Table 4.

3. Experimental Setup

3.1 Development of PID and fuzzy PID Simulink models

On the basis of the obtained transfer functions for the pitch angle θ and horizontal stabilizer deflection δe of the micro-sized electric UAV in this study, as shown in Eq. (7), traditional PID

Table 4
Fuzzy rules.

e	*ec*						
	NB	NM	NS	ZO	PS	PM	PB
NB	PB/NB/PS	PB/NB/NS	PM/NM/NB	PM/NM/NB	PS/NS/NB	ZO/ZO/NM	ZO/ZO/PS
NM	PB/NB/PS	PB/NB/NS	PM/NM/NB	PS/NS/NM	PS/NS/NM	ZO/ZO/NM	NS/ ZO/ZO
NS	PM/NB/ZO	PM/NM/NS	PM/NS/NM	PS/NS/NM	ZO/ZO/NS	NS/PS/NS	NS/PS/ZO
ZO	PM/NB/ZO	PM/NM/NS	PS/NS/NS	ZO/ZO/NS	NS/PS/NS	NM/PM/NS	NM/PM/ZO
PS	PS/ZO/PB	ZO/ZO/NS	NS/PS/PS	NM/PS/PS	NM/PM/PS	NM/PB/PS	NB/PB/PB
PM	ZO/ZO/PB	ZO/ZO/PM	NM/PS/NS	NM/PM/PM	NM/PM/PS	NB/PB/PS	NB/PB/PB

and fuzzy PID controller models were constructed using Simulink for tests and performance comparison, as depicted in Fig. 5.

3.2 Power source and battery selection for micro-sized electric UAV

The electric UAV weighs 1250 g in this study, as indicated in Table 1. Before actual UAV flight tests are conducted, it is essential to first determine an appropriate motor thrust. From the design principles of electric UAV thrust,[26] the initial set ratio of thrust to total UAV weight must exceed 0.8 (thrust/weight > 0.8). In this study, a brushless DC motor was chosen as the power source for the UAV owing to its lightweight and high thrust characteristics. The selected motor with model number 2814/1250KV is produced by LangYu Company. When paired with a 6-inch propeller, it can generate a thrust of 1750 g, as detailed in Table 5. A motor thrust exceeding the total weight provides sufficient power for propelling the UAV.

To ensure sufficient power supply for the electric UAV and to guarantee stability during the tests, we utilized a lithium polymer (Li–Po) battery.[27–29] The battery specifications were as follows: a voltage of 12.5 V, a current of 3300 mA, a maximum discharge rate of 35 C, a maximum instantaneous discharge current of 57 amperes, a power rating of 720 W, and a weight of 146 grams. This Li–Po battery is designed specifically for lightweight and high-power micro-sized electric UAVs, providing a safe flight time of 6 min.

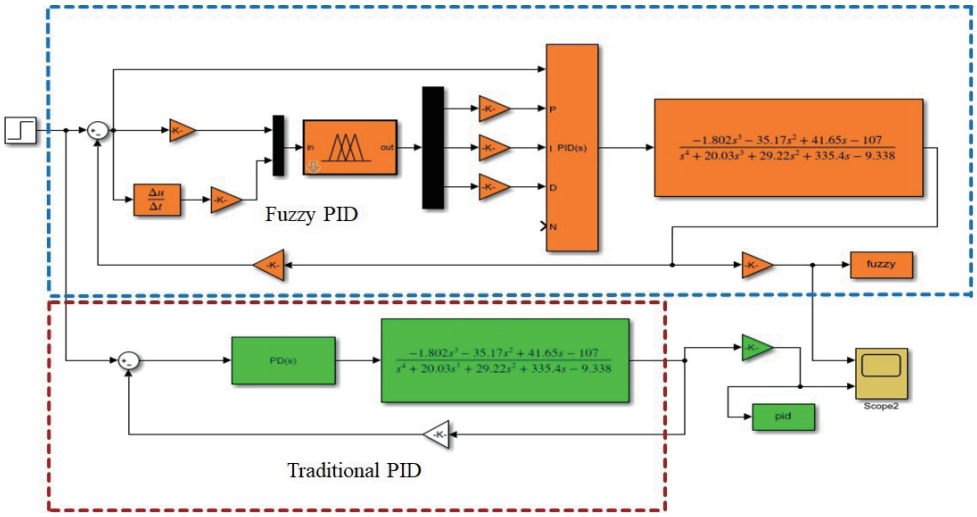

Fig. 5. (Color online) PID and fuzzy PID Simulink.

Table 5
Specifications of 2814/1250KV brushless DC motor.

Volts	Amps	Thrust	Watts	Weight
12.5 V	33 A	1750 g	750 W	113 g

3.3 Flight tests of micro-sized electric UAV

Our ground station for UAV flight utilized the widely used Mission Planner (MP) software for flight control tests and observation. The flight test location was situated at a longitude of 120.5406889 and a latitude of 24.2651959, with a temperature of 28 ºC and a wind speed of 3.6 m/s. Initially, the UAV's flight conditions were configured using the MP software, including elevator control angles of ±5º and a maximum cruising speed set at 13 m/s. Upon takeoff, the UAV was operated in Auto Cruise mode for test purposes. To set the flight speed of the UAV, a dedicated set of sensors, specifically Pitot tubes, need to be installed on the UAV's flight control computer, as shown in Fig. 6. This setup assists the UAV in maintaining the correct flight speed.

4. Result

4.1 Simulink simulation results of micro-sized electric UAV's longitudinal controller

Under the requirements and indices for UAV flight control, including settling time, overshoot, peak time, and rise time, as presented in Table 6, the initial flight simulation was conducted using traditional PID parameters as inputs in Simulink. This study's simulation process involved a comparative analysis using fuzzy PID and traditional PID controllers and comparisons with

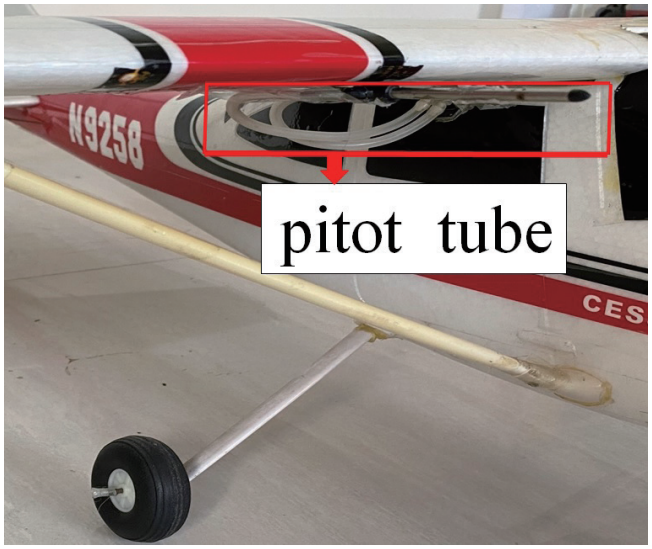

Fig. 6. (Color online) Airspeed sensor - Pitot tube.

Table 6
Default flight control requirements and indices.

Item	Target
Settling time	<4 s
Overshoot	<60 %
Peak time	<2 s
Rise time	<1 s

studies that used only traditional PID[11] and fuzzy PID[12,13] controllers for simulated flight. The superior flight stability performance in this study was demonstrated through the evaluation of rise time, peak time, overshoot, and settling time. The simulated flight test results obtained in this research, as illustrated in Fig. 7, were compared with the predefined requirements in Table 7. The simulated flight results indicated that the traditional PID controller did not meet the expected objectives.

In the second simulation, fuzzy theory was utilized, and a fuzzy rule table designed specifically for this research, as shown in Table 5, was employed to address the shortcomings of the traditional PID controller. A comparison was made with the traditional PID controller, as depicted in Fig. 8. The simulated flight results demonstrated improved efficiency and compliance with the expected objectives, as summarized in Table 7.

The first flight test was conducted using traditional PID parameters input into the flight control computer, and the results are presented in Fig. 8. The second test utilized Fuzzy PID parameters input into the flight control computer, with results shown in Fig. 9.

4.2 Results of practical flight tests for micro-sized electric UAV

UAVs exhibit primary flight modes such as takeoff, climbing, cruising, and landing. Within the initial 2 min of UAV takeoff, the longitudinal state of the aircraft becomes unstable. This instability is primarily attributed to the transition of the UAV from a stationary position to a fixed altitude flight, involving takeoff and climb flight modes. The pitch angle of the UAV

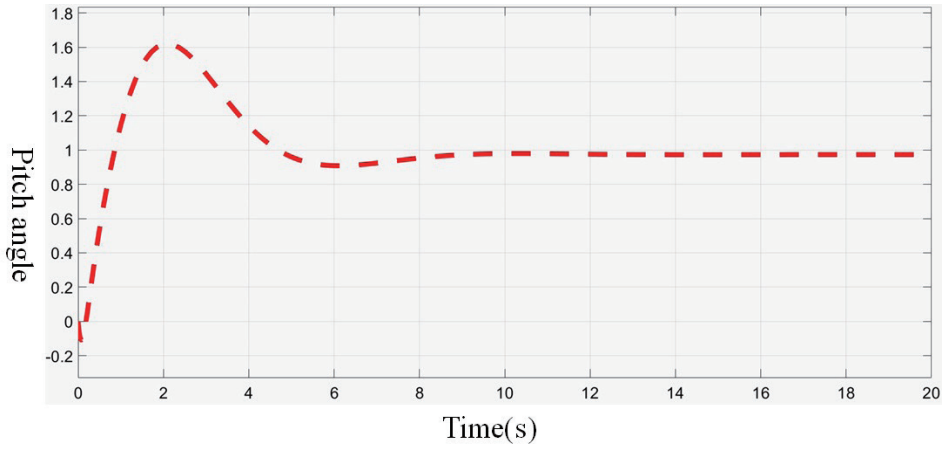

Fig. 7. (Color online) Traditional PID controller results (simulated flight tests).

Table 7
Comparison of traditional PID and fuzzy PID controllers.

Item	Target	Traditional PID	Fuzzy PID	Enhanced efficiency
Settling time	<4 s	8.12 s	2.71 s	66.7%
Overshoot	<60%	67.7%	52.2%	23%
Peak time	<2 s	2.17 s	0.17 s	92.1%
Rise time	<1 s	0.51 s	0.07 s	86.2%

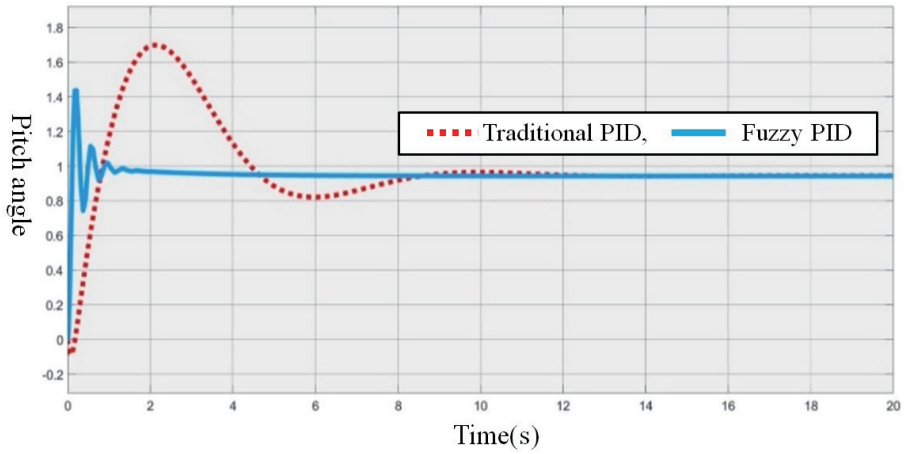

Fig. 8. (Color online) Comparison between traditional PID and fuzzy PID (simulated flight tests).

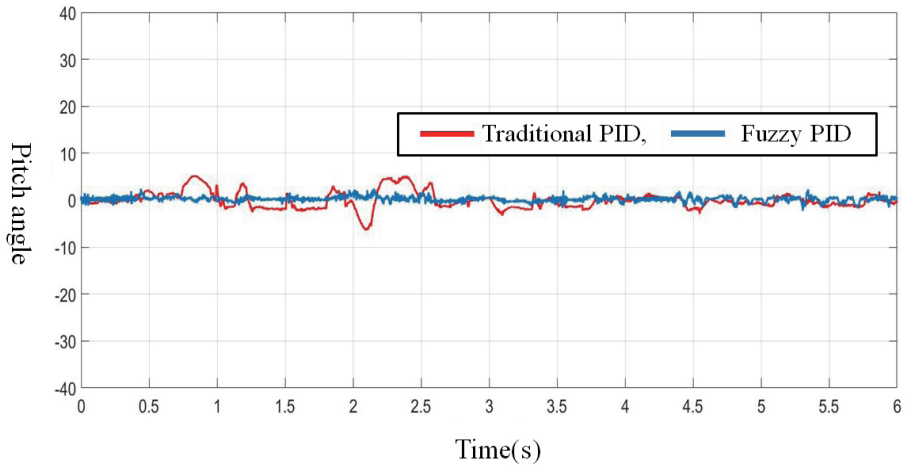

Fig. 9. (Color online) Observations of micro-sized electric UAV flight (actual flight tests).

contributes to this longitudinal instability. To empirically verify the impact of traditional PID and fuzzy PID control systems on actual flight, we conducted a comparative analysis using results of real flight test.[14,30] The results from these real flight tests indicated that fuzzy PID significantly enhances the longitudinal flight stability of fixed-wing UAVs. We observed the longitudinal state of the UAV from the 2nd to the 6th min. Our observations indicated that the implementation of fuzzy PID control, as compared with traditional PID control, enhances the adaptive and robust characteristics of micro-sized electric UAVs, as illustrated in Fig. 9.

5. Conclusion and Summary

Our main objective was to enhance the stability of longitudinal flight in micro-sized electric UAVs. This was motivated by the fact that the traditional PID controller is one of the most widely used controllers today owing to its simple structure, ease of design, and excellent robustness.

However, the drawback of PID controllers is their limited suitability for nonlinear systems. In contrast, the fuzzy PID controller exhibits good adaptability and robustness and performs effectively in nonlinear systems. We conducted a comparative analysis of various performance indicators for both controllers: (1) Settling time: The traditional PID controller requires 8.12 s, whereas the fuzzy PID controller requires 2.71 s, resulting in a 66.7% improvement in efficiency when comparing the two. (2) Overshoot: With the traditional PID controller, there is a 67.7% overshoot, whereas the fuzzy PID controller exhibits a 52.2% overshoot, resulting in a 23% improvement in efficiency. (3) Peak time: The traditional PID controller requires 2.17 s, whereas the fuzzy PID controller only needs 0.17 s, resulting in a remarkable 92.1% improvement in efficiency. (4) Rise time: The traditional PID controller achieves a rise time of 0.51 s, whereas the fuzzy PID controller achieves it in 0.07 s, indicating an 86.2% improvement in efficiency when comparing the two.

The simulated flight test results have confirmed that the fuzzy PID controller is more efficient than the traditional PID controller in enhancing the adaptive and robust characteristics of UAVs. In this study, the designed fuzzy PID controller parameters were linked to the flight control computer, and the feasibility of using the fuzzy PID control was verified through actual flight tests of a UAV. By observing the longitudinal state of the UAV, we aimed to demonstrate that fuzzy PID control, as compared with the traditional PID control, enhances the adaptive and robust characteristics of micro-sized electric UAVs. The integration of neural networks with fixed-wing UAVs can significantly broaden their future applications, holding substantial potential across various sectors, particularly in the military domain, where they are expected to play a pivotal role in reconnaissance, surveillance, and intelligence operations.

References

1 M. Tao, X. Li, H. Yuan, and W. Wei: Inf. Sci. **532** (2020) 155. https://doi.org/10.1016/j.ins.2020.03.053
2 B. Xu, D. Chen, M. Venkateshkumar, Y. Xiao, Y. Yue, Y. Xing, and P. Li: Appl. Energy **248** (2019) 446. https://doi.org/10.1016/j.apenergy.2019.04.125
3 G. Mariscal, C. Depcik , H. Chao, G. Wu, and X. Li: Energy Convers. Manage. **301** (2024) 118005. https://doi.org/10.1016/j.enconman.2023.118005
4 M. Dorigo, M. Birattari, and T. Stutzle: IEEE Comput. Intell. Mag. **1** (2006) 28. https://doi.org/10.1109/MCI.2006.329691
5 D. Jain, S. Neelakandan, T. Veeramani, S. Bhatia, and F. H. Memon: Comput. Electr. Eng. **102** (2022) 108135. https://doi.org/10.1016/j.compeleceng.2022.108135
6 X. Liu, X. Du, X. Zhang, Q. Zhu, and M Guizani: Comput. Electr. Eng. **80** (2019) 106493. https://doi.org/10.1016/j.compeleceng.2019.106493
7 L. Tan, X. Lv, X. Lian, and G. Wang: Comput. Electr. Eng. **93** (2021) 107261: https://doi.org/10.1016/j.compeleceng.2021.107261
8 K. Robindro, S. S. Devi, U. B. Clinton, L. Takhellambam, Y. R. Singh, and N. Hoque: Comput. Electr. Eng. **7** (2024) 64. https://doi.org/10.1016/j.dsm.2023.10.003
9 M. Hermassi, S. Krim, Y. Kraiem, and M. A. Hajjaji: Comput. Electr. Eng. **117** (2024) 109264. https://doi.org/10.1016/j.compeleceng.2024.109264
10 Z. Liu, Z. Liu, J. Liu, and N. Wang: Appl. Energy **352** (2023) 121936. https://doi.org/10.1016/j.apenergy.2023.121936
11 J. M. Levina, A. A. Paranjapeb, and M. Nahon: Rob. Auton. Syst. **116** (2019) 148. https://doi.org/10.1016/j.robot.2019.03.004
12 L. Chu, Q. Li, F. Gu, X. Du, Y. He, and Y. Deng: Chin. J. Aeronaut. **35** (2022) 2020. https://doi.org/10.1016/j.cja.2021.09.013
13 L. Yan, J. L. Webber, A. Mehbodniya, B. Moorthy, S. Sivamani, S. Nazir, and M. Shabaz: Comput. Electr. Eng. **101** (2022) 108059. https://doi.org/10.1016/j.compeleceng.2022.108059

14 R. Sun, Z. Zhou, and X. Zhu: Aerosp. Sci. Technol. **120** (2022) 107263. https://doi.org/10.1016/j.ast.2021.107263
15 J. Kim, S. Kim, C. Ju, and H. Son: IEEE Access **7** (2019) 105100. https://doi.org/10.1109/ACCESS.2019.2932119
16 P. R. Grammatikis, P. Sarigiannidis, T. Lagkas, and I. Moscholios: Comput. Networks **172** (2020) 107148. https://doi.org/10.1016/j.comnet.2020.107148
17 X. Yan, J. Zhu, M. Kuang, and X. Wang: Aerosp. Sci. Technol. **86** (2019) 826. https://doi.org/10.1016/j.ast.2019.02.003
18 Y. H. Hou, X. Liang, and X. Y. Mu: Int. J. Nav. Archit. Ocean Eng. **10** (2018) 499. https://doi.org/10.1016/j.ijnaoe.2017.10.001
19 J. Li, Y. Yao, D. Jia, C. Ge, Z. Wang, and T. Yang: Opt. Commun. **569** (2024) 130824. https://doi.org/10.1016/j.optcom.2024.130824
20 S. Yun, N. Fu, and L. Qiao: Digital Signal Process. **148** (2024) 104435. https://doi.org/10.1016/j.dsp.2024.104435
21 N. Tan, I. Kaya, C. Yeroglu, and D. P. Atherton: Energy Convers. Manage. **47** (2006) 3045. https://doi.org/10.1016/j.enconman.2006.03.022
22 M. T. Söylemez, N. Munro, and H. Baki: Automatica **39** (2003) 121. https://doi.org/10.1016/S0005-1098(02)00180-2
23 K. Nanavati, M. Gupta, and B. Jayaram: Fuzzy Sets Syst. **490** (2024) 109040. https://doi.org/10.1016/j.fss.2024.109040
24 S. J. Fong, G. Li, N. Dey, R. G. Crespo, and E. H. Viedma: Appl. Soft Comput. **93** (2020) 106282. https://doi.org/10.1016/j.asoc.2020.106282
25 M. Hasanipanah and H. B. Amnieh: Nat. Resour. Res. **29** (2020) 669. https://doi.org/10.1007/s11053-020-09616-4
26 J. Burgués and S. Marco: Sci. Total Environ. **748** (2020) 141172. https://doi.org/10.1016/j.scitotenv.2020.141172
27 D. Çalışır, S. Ekici, A. Midilli, and T. H. Karakoc: Energy **262** (2023) 125543. https://doi.org/10.1016/j.energy.2022.125543
28 N. Eleftheroglou, S. S. Mansouri, T. Loutas, P. Karvelis, G. Georgoulas, G. Nikolakopoulos, and D. Zarouchas: Appl. Energy **254** (2019) 113677. https://doi.org/10.1016/j.apenergy.2019.113677
29 C. Depcik, T. Cassady, B. Collicott, S. P. Burugupally, X. Li, S. S. Alam, J. R. Arandia, and J. Hobeck: Energy Convers. Manage. **207** (2020) 112514. https://doi.org/10.1016/j.enconman.2020.112514
30 K. Watanabe, T. Shibata, and M. Ueba: Aerospace **11** (2024) 233. https://doi.org/10.3390/aerospace11030233

About the Authors

Chao-Pang Wu received his B.S. degree in electrical engineering from National Taipei University of Technology in Taiwan and obtained a doctoral candidate qualification from the Department of Electrical Engineering of Changhua Normal University in 2023. His research interests are in aerospace, electrical engineering, and sensors.

Nan-Kai Hsieh received his Ph.D. degree from the Department of Mechanical Engineering of National Taiwan University, Taipei, Taiwan, in 2015. He has been an assistant professor at Feng Chia University since 2022. His interests spans many professional fields, including prognostic and health management (PHM), mechatronics, robot vision, and IoT.

Liang-Rui Chen received his B.S., M.S., and Ph.D. degrees in electronic engineering from National Taiwan University of Science and Technology, Taipei, Taiwan, in 1994, 1996, and 2001, respectively. He joined the faculty of the Department of Electrical Engineering, National Changhua University of Education, Changhua, in August 2006, where he is currently a professor. His primary research interests include power electronics and automatic control.